

Light-induced odd-parity altermagnets on dimerized lattices

Dongling Liu,^{1,*} Zheng-Yang Zhuang,^{1,*} Di Zhu,^{1,*} Zhigang Wu,^{2,†} and Zhongbo Yan^{1,‡}

¹*Guangdong Provincial Key Laboratory of Magnetoelectric Physics and Devices,
State Key Laboratory of Optoelectronic Materials and Technologies,
School of Physics, Sun Yat-sen University, Guangzhou 510275, China*

²*Quantum Science Center of Guangdong-Hong Kong-Macao Greater Bay Area (Guangdong), Shenzhen 508045, China
(Dated: August 27, 2025)*

Altermagnets are an emerging class of collinear magnets with momentum-dependent spin splitting and zero net magnetization. These materials can be broadly classified into two categories based on the behavior of spin splitting at time-reversal-related momenta: even-parity and odd-parity altermagnets. While even-parity altermagnets have been thoroughly investigated both theoretically and experimentally, the systems capable of hosting odd-parity altermagnetism remain largely unexplored. In this work, we demonstrate that circularly polarized light dynamically converts collinear \mathcal{PT} -symmetric antiferromagnets on dimerized lattices into odd-parity p -wave altermagnets. Because of the underlying Dirac band structure of the dimerized lattice, we find that the resulting p -wave altermagnets can realize Chern insulators (2D) and Weyl semimetals (3D) under appropriate drive conditions. Our findings demonstrate that collinear antiferromagnets on dimerized lattices provide ideal platforms to investigate the dynamical generation of odd-parity altermagnetism.

Altermagnets (AMs), a recently discovered class of collinear compensated magnets, have attracted significant attention for combining the advantageous features of ferromagnets and antiferromagnets [1–24]. Their defining characteristic is momentum-dependent spin splitting (MDSS) in the band structure despite zero net magnetization and the absence of spin-orbit coupling (SOC), necessitating the existence of nodal planes across which the spin splitting reverses sign. Based on the rotation angle between adjacent nodal planes, these systems are classified as d -, g -, and i -wave AMs [1]. All of them share a unified electronic structure: $E(\mathbf{k}, s) \neq E(\mathbf{k}, -s)$ for generic momenta \mathbf{k} while maintaining $E(\mathbf{k}, s) = E(-\mathbf{k}, s)$ (s denotes spin). This symmetry classifies them as even-parity AMs since the MDSS is even under inversion (\mathcal{P}). Such even-parity MDSS enables numerous extraordinary phenomena, such as anisotropic tunneling phenomena[25–30], finite-momentum Cooper pairing [31–35], unconventional superconductivity[36–45], and diverse topological phases [45–57], making materials with MDSS promising candidates for next-generation spintronics and quantum computing applications.

MDSS in magnets can also be odd under inversion. This demands that the energy bands satisfy the relation: $E(\mathbf{k}, s) = E(-\mathbf{k}, -s)$. The existence of this energy relation in magnets is remarkable because it typically arises from time-reversal symmetry (TRS), yet this symmetry is explicitly broken in magnets. Although relativistic SOC can generate this effect, the pursuit of nonrelativistic mechanisms is of fundamental interest. One proposed route involves interaction-driven Fermi surface instabilities [58–63], though its experimental realization remains elusive, possibly for fundamental reasons [64, 65]. Alternatively, recent spin group theory has established that odd-parity MDSS can arise at the single-particle level in coplanar magnets that lack inversion symmetry but preserve the combined time-reversal-translation symmetry ($\mathcal{T}\tau$) [66]. This discovery has led to the conception of p -wave magnets [66] and their higher-partial-wave gener-

alizations [67]. Remarkably, experimental evidence for odd-parity MDSS in such coplanar magnets has recently been reported [68], demonstrating a viable nonrelativistic mechanism for its realization.

The odd-parity MDSS in these coplanar magnets exhibits two key features [66, 67, 69, 70]: (1) it is confined to the spin component perpendicular to the moment plane, satisfying $\langle s_{\perp}(\mathbf{k}) \rangle = -\langle s_{\perp}(-\mathbf{k}) \rangle$; and (2) the spin polarization, being non-conserved, displays strong momentum dependence. Thus, it requires precise Fermi energy or optical frequency tuning to access the regions of significant polarization, severely limiting potential applications. A more favorable scenario would involve realizing odd-parity MDSS in collinear magnets. Remarkably, this is possible. While earlier spin group theory has only identified even-parity AMs, this conclusion originated from the assumption that the underlying nonmagnetic crystal structures preserve TRS. Recently, Lin revealed that if TRS is preemptively broken by sublattice currents, the subsequent emergence of collinear antiferromagnetic order in a bipartite lattice can realize odd-parity MDSS [71]. This discovery defines odd-parity p - and f -wave AMs, distinct from even-parity and noncollinear types.

Sublattice currents demand a delicate real-space flux distribution, a condition that is challenging to realize in actual materials, as exemplified by the celebrated Haldane model [72]. Interestingly, circularly polarized light (CPL) offers a direct and versatile alternative to break TRS. Furthermore, when applied to systems with a Dirac band structure, CPL can dynamically induce topologically non-trivial phases, such as 2D Chern insulators [73–77] and 3D Weyl semimetals [78–84]. Therefore, irradiating collinear antiferromagnets with CPL could serve as a generic approach for engineering odd-parity AMs with nontrivial topological properties, a mechanism recently demonstrated in 2D honeycomb-lattice systems by three independent groups [85–87]. Here, we implement this approach in 2D and 3D collinear antiferromagnets on dimerized lattices, relevant to strongly correlated materials

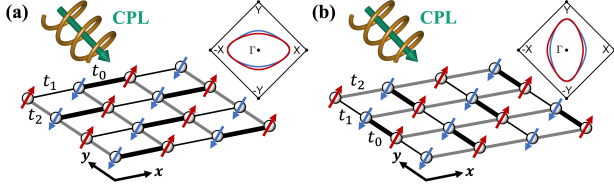


FIG. 1. Schematic of a collinear antiferromagnet on a 2D dimerized lattice under CPL irradiation. Red and blue arrows on the lattice represent magnetic moments of opposite directions. Thick (black) solid lines denote the bonds of dimerization. (a) When dimerization occurs along the x direction (type-I), the Fermi surfaces with opposite spins undergo opposite shifts along the y direction. (b) When dimerization is oriented along the y direction (type-II), the spin-split Fermi surfaces instead shift oppositely along the x direction.

like cuprates [88, 89]. We demonstrate that CPL drives the system into an odd-parity p -wave AM. The resulting MDSS is tunable via the handedness and incident direction of the CPL and emerges consistently along axes (2D) or in planes (3D) perpendicular to the dimerization. Above a threshold intensity, the system transitions into an altermagnetic Chern insulator (2D) or altermagnetic Weyl semimetal (3D).

2D collinear antiferromagnets on dimerized lattices.—We examine two dimerization configurations related by a $\pi/2$ rotation, aiming to show that the induced odd-parity MDSS exhibits a nontrivial dependence on the dimerization direction, as illustrated in Fig. 1. The single-particle Hamiltonian describing spin- $\frac{1}{2}$ fermions propagating on these dimerized lattices under the magnetic background is given by

$$H = \sum_{\langle ij \rangle} t_{ij} c_i^\dagger c_j + \sum_i \xi_i c_i^\dagger (\mathbf{M} \cdot \mathbf{s}) c_i, \quad (1)$$

where $c_i = (c_{i,\uparrow}, c_{i,\downarrow})^T$ with $c_{i,s}$ ($c_{i,s}^\dagger$) denoting the annihilation (creation) operator for a fermion at site i and with spin s . Here t_{ij} denotes the hopping constants between two nearest-neighbor sites i and j , which are parameterized by t_0 , t_1 and t_2 for our dimerized model (see the illustration in Fig. 1). The exchange field induced by antiferromagnetic order is given by the vector $\mathbf{M} = (M_x, M_y, M_z)$, while $\mathbf{s} = (s_x, s_y, s_z)$ denotes the vector of Pauli matrices in spin space. The sublattice degree of freedom is encoded by ξ_i , where $\xi_i = 1(-1)$ for sublattice A (B), reflecting the staggered nature of the antiferromagnetic order.

By Fourier transform, the corresponding momentum-space Hamiltonian for the type-I dimerization configuration shown in Fig. 1(a) is obtained as

$$\mathcal{H}^{(I)}(\mathbf{k}) = (t_+ \cos k_x + 2t_2 \cos k_y) \sigma_x + t_- \sin k_x \sigma_y + \mathbf{M} \cdot \mathbf{s} \sigma_z, \quad (2)$$

where the Pauli matrices σ_i act on the two sublattice degrees of freedom, and the parameters $t_\pm = t_0 \pm t_1$. For notational simplicity, we set the lattice constants to unity, omit identity matrices, and assume all three hopping parameters (t_0 , t_1 and t_2) to be positive constants throughout this work.

The Hamiltonian for the type-II dimerization configuration can be obtained from the type-I Hamiltonian through the relation $\mathcal{H}^{(II)}(k_x, k_y) = \mathcal{H}^{(I)}(k_y, -k_x)$. Given this straightforward mapping, we will focus our analysis on $\mathcal{H}^{(I)}(\mathbf{k})$ in the following discussion.

In the absence of antiferromagnetic order ($\mathbf{M} = 0$), the Hamiltonian describes AB-stacked Su-Schrieffer-Heeger (SSH) chains [90] along the y direction. In the weak-coupling regime ($t_2 \ll t_+$), the system forms a weak topological insulator exhibiting flat-band edge states exclusively on x -normal edges. These flat bands float within the bulk gap and span the entire boundary Brillouin zone. Conversely, in the strong-coupling regime ($t_2 \gg t_+$), the system becomes a Dirac semimetal that also supports flat bands on x -normal edges. However, these flat bands terminate at the projections of bulk Dirac points and thus only occupy a portion of the boundary Brillouin zone. In what follows, we focus on the regime with $t_2 > t_+/2$, corresponding to a Dirac semimetal when $\mathbf{M} = 0$.

The Dirac points in the 2D SSH model are protected by spinless \mathcal{PT} symmetry, where the symmetry operator is given by $\mathcal{PT} = \sigma_x \mathcal{K}$ (with \mathcal{K} representing the complex conjugation operator) and satisfies $(\mathcal{PT})^2 = 1$. However, this symmetry is broken when the antiferromagnetic order is introduced. Consequently, energy gaps open at the Dirac points, driving the system into an antiferromagnetic insulating phase. The antiferromagnetic insulator has spin-degenerate energy bands as the Hamiltonian $\mathcal{H}^{(I)}(\mathbf{k})$ possesses a spinful \mathcal{PT} symmetry, where the symmetry operator is given by $\mathcal{PT} = \sigma_x s_y \mathcal{K}$. This symmetry operator satisfies $(\mathcal{PT})^2 = -1$, thereby enforcing Kramers degeneracy throughout the spectrum.

Floquet p -wave altermagnetic Chern insulator.—Now we explore the influence of CPL on the system. Consider light incident perpendicular to the plane of the 2D system, described by the vector potential $\mathbf{A}(t) = A_0(\cos \omega t, \eta \sin \omega t)$, where $\eta = +1$ and $\eta = -1$ correspond to right-handed and left-handed CPL, respectively. The electromagnetic coupling is given by $\mathcal{H}^{(I)}(\mathbf{k}) \rightarrow \mathcal{H}^{(I)}[\mathbf{k} + \mathbf{A}(t)]$ (we set $e = \hbar = 1$ for notational simplicity). Since the Hamiltonian becomes time-periodic, it can be expanded in a Fourier series as $\mathcal{H}^{(I)}[\mathbf{k} + \mathbf{A}(t)] = \sum_n \mathcal{H}_n(\mathbf{k}) e^{in\omega t}$ with $n \in \mathbb{Z}$. We focus on the high-frequency off-resonant regime, where the driven system is effectively described by a time-independent Hamiltonian given by [74, 91]

$$\mathcal{H}_{\text{eff}}(\mathbf{k}) = \mathcal{H}_0(\mathbf{k}) + \sum_{n \geq 1} \frac{[\mathcal{H}_{+n}, \mathcal{H}_{-n}]}{n\omega} + O(\omega^{-2}). \quad (3)$$

Keeping the leading-order contributions, we find

$$\mathcal{H}_{\text{eff}}(\mathbf{k}) = J_0(A_0)[(t_+ \cos k_x + 2t_2 \cos k_y) \sigma_x + t_- \sin k_x \sigma_y] + \mathbf{M} \cdot \mathbf{s} \sigma_z - \eta F(A_0, \omega) \sin k_y \cos k_x \sigma_z, \quad (4)$$

where $J_n(x)$ is the n -th order Bessel function of the first kind, and $F(A_0, \omega) = 8J_1^2(A_0)t_2 t_- / \omega$. Compared to the original static Hamiltonian, the key modification induced by CPL is the emergence of the last term. This term breaks the

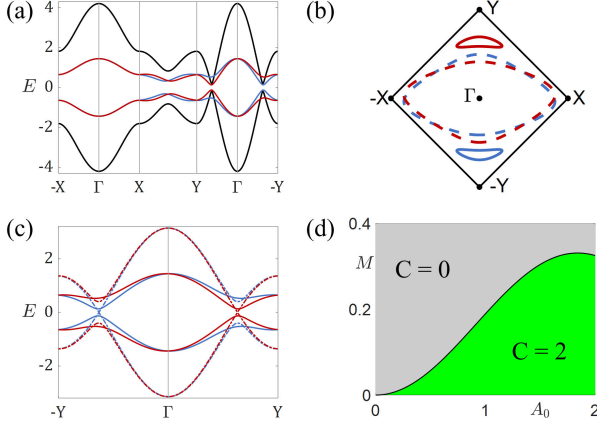


FIG. 2. (a) Energy bands of the static (black, spin-degenerate) and CPL-driven ($A_0 = 1.8$, red/blue for spin up/down) systems. (b) Fermi surface at Fermi energy $E_F = 0.2$ (solid lines) and $E_F = 0.7$ (dashed lines), corresponding to the light-induced spin split bands in (a). (c) Band gap evolution: closure at the critical drive (dashed, $A_0 = 1.04$) and reopening for a stronger drive (solid, $A_0 = 1.8$). (d) Topological phase diagram in the (M, A_0) plane. The value $M = 0.2$ is used in (a-c). Shared parameters for all panels are $t_0 = 1$, $t_1 = 0.2$, $t_2 = 1.5$, $\eta = 1$, and $\omega = 9$.

spinful \mathcal{PT} symmetry of the static Hamiltonian, thereby lifting the spin degeneracy in the band structure. Notably, this term exhibits odd-parity momentum dependence, which is essential for generating odd-parity MDSS. We emphasize that this term arises from the interplay between the $\cos k_y \sigma_x$ and $\sin k_x \sigma_y$ terms in the time-periodic Hamiltonian. Three key features of these two terms—their anticommutation relation, dependence on orthogonal momenta, and opposite parity under momentum inversion (even vs odd)—are responsible for producing terms with the desired odd-parity momentum dependence. Importantly, terms fulfilling these three conditions appear generically in dimerized systems, suggesting the universality of this mechanism.

Although both TRS and spinful \mathcal{PT} symmetry are broken, the driven system maintains compensated magnetization. This compensation arises from the preserved $[C_{2\perp} \parallel \mathcal{P}]$ symmetry in the driven Hamiltonian, where $C_{2\perp}$ denotes a π rotation in the spin space around an axis perpendicular to the Néel vector, and \mathcal{P} denotes the spatial inversion operation. This symmetry guarantees the energy relation $E(\mathbf{k}, s) = E(-\mathbf{k}, -s)$, which explicitly forbids net magnetization. Notably, $[C_{2\perp} \parallel \mathcal{P}]$ imposes the same constraint on energy bands as TRS. Consequently, when spin splitting occurs, it must exhibit an odd-parity pattern—analogueous to that induced by SOC.

Given the system's rotational invariance with respect to the Néel vector orientation, we hereafter fix the Néel vector along the z direction, i.e., $\mathbf{M} = M\hat{z}$ with $M > 0$. In Fig. 2(a), we show a comparison of the band structure with and without CPL irradiation. In the static case, the spin-up and spin-down energy bands are degenerate. Under CPL driving, however, a clear spin splitting emerges in the band structure. This split-

ting exhibits two key features: odd-parity nature and strong anisotropy. The odd-parity feature is evident in the energy spectrum along the k_y axis ($-Y-\Gamma-Y$). The anisotropy is manifested as a stark contrast in the energy spectrum between k_x ($-X-\Gamma-X$) and k_y axes: the splitting is strongest along k_y but entirely absent along k_x . In Fig. 2(b), we present Fermi surfaces at two distinct Fermi energies (E_F). The spin-up and spin-down Fermi surfaces are clearly related by the $[C_{2\perp} \parallel \mathcal{P}]$ symmetry, confirming its key role in the system.

Assuming that the CPL irradiation does not modify the antiferromagnetic order, we note that increasing the light amplitude can induce a closing and reopening of the bulk energy gap, as illustrated in Fig. 2(c). This gap close triggers a topological phase transition from a trivial insulator to a Chern insulator characterized by Chern number $|C| = 2$. To intuitively understand this transition, we perform a low-energy expansion near the momentum where the gap close occurs. Such momenta are at $\mathbf{k}_{D,\pm} = \pm(0, \pi - \arccos(t_+/2t_2))$ (we assumed $t_2 > t_+/2$). Near these two momenta, the low-energy Hamiltonian is given by

$$\mathcal{H}_{\chi,s}(\mathbf{q}) = -\chi v_y q_y \sigma_x + v_x q_x \sigma_y + (sM - \chi\eta\tilde{F})\sigma_z. \quad (5)$$

Here, $\chi = \pm 1$ indexes the two valleys located at $\mathbf{k}_{D,\pm}$, while $s = \pm 1$ corresponds to the spin-up and spin-down sectors, respectively. The small momentum $\mathbf{q} = (q_x, q_y)$ is measured relative to $\mathbf{k}_{D,\pm}$. For notation convenience, we introduce the following definitions: $v_x = J_0(A_0)t_-$, $v_y = J_0(A_0)\sqrt{4t_2^2 - t_+^2}$, and $\tilde{F} = F(A_0, \omega)\sqrt{4t_2^2 - t_+^2}/2t_2$.

Since the \mathcal{PT} symmetry guarantees that the pre-driving Hamiltonian has $C = 0$, the system remains topologically trivial before the energy gap closes. When the gap reopens, the Chern number of the driven system can be determined by tracking its change through the gap-closing transition, as captured by the low-energy Hamiltonians. The Chern numbers for those low-energy Hamiltonian are given by [92]

$$C_{\chi,s} = -\frac{1}{4\pi} \int dq_x \int dq_y \frac{\mathbf{h}_{\chi,s} \cdot (\partial_{q_x} \mathbf{h}_{\chi,s} \times \partial_{q_y} \mathbf{h}_{\chi,s})}{|\mathbf{h}_{\chi,s}|^3}, \quad (6)$$

where $\mathbf{h}_{\chi,s} = (-\chi v_y q_y, v_x q_x, sM - \chi\eta\tilde{F})$. Direct calculation yields: $C_{\chi,s} = \text{sgn}(\eta\tilde{F} - \chi s M)/2$, where $\text{sgn}(x)$ is the sign function (+1 for $x > 0$ and -1 for $x < 0$). Two of these Chern numbers undergo a sudden change when \tilde{F} crosses the critical value M at which the bulk energy gap closes. Specially, the changes in Chern number satisfy $\Delta C_{+,\uparrow} = \Delta C_{-,\downarrow} = (1 + \eta)/2$ and $\Delta C_{-,\uparrow} = \Delta C_{+,\downarrow} = (\eta - 1)/2$, which are also a consequence of the $[C_{2\perp} \parallel \mathcal{P}]$ symmetry. Accordingly, the Chern number characterizing the system in the region $\tilde{F} > M$ is derived as $C = 2\eta$, which is controlled by the CPL's handedness. This analysis fully determines the topological phase diagram shown in Fig. 2(d).

The emergence of gapless chiral edge states constitutes a defining signature of Chern insulators. Our calculations of the energy spectrum for cylindrical-geometry samples demonstrate two branches of gapless chiral edge states in the $\tilde{F} > M$

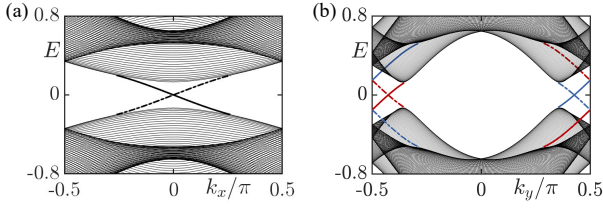


FIG. 3. Energy spectrum for a sample of cylindrical geometry. (a) y -normal edges: Spin-degenerate spectrum of chiral edge states. States on the bottom (top) edge are shown as solid (dashed) lines. (b) x -normal edges: Spin-split spectrum of chiral edge states. States on the left (right) edge are shown as solid (dashed) lines. Parameters are $t_0 = 1$, $t_1 = 0.2$, $t_2 = 1.5$, $M = 0.2$, $\eta = 1$, $A_0 = 1.8$, and $\omega = 9$.

regime, confirming the predicted bulk topological invariant. Strikingly, these edge states inherit the bulk's anisotropic spin splitting: while remaining spin-degenerate along y -normal edges (where k_x is conserved), they develop pronounced spin splitting along x -normal edges (with conserved k_y), as clearly evidenced in Figs. 3(a) and 3(b).

Floquet p -wave altermagnetic Weyl semimetals.—The 2D scenario admits a natural extension to 3D. As a prototypical example, we construct a 3D system by AB-stacking identical copies of the 2D Hamiltonian along the z axis [illustrated in Fig. 4(a)], obtaining the following static Hamiltonian:

$$\mathcal{H}^{3D}(\mathbf{k}) = (t_+ \cos k_x + 2t_2 \cos k_y + 2t_3 \cos k_z)\sigma_x + t_- \sin k_x \sigma_y + M s_z \sigma_z, \quad (7)$$

where t_3 is the interlayer hopping constant. Interestingly, we find that the orientation of incident light has a strong impact on the spin-splitting features in 3D. To demonstrate this, we consider that the light is incident along a general direction, described by $\mathbf{n} = (\cos \phi \sin \theta, \sin \phi \sin \theta, \cos \theta)$, where ϕ and θ are the azimuthal and polar angles on the Bloch sphere, respectively. The vector potential of the light is given by $\mathbf{A}(t) = A_0[\cos(\omega t)\mathbf{e}_1 + \eta \sin(\omega t)\mathbf{e}_2]$, where $\mathbf{e}_1 = (\sin \phi, -\cos \phi, 0)$ and $\mathbf{e}_2 = (\cos \phi \cos \theta, \sin \phi \cos \theta, -\sin \theta)$, corresponding to two unit orthogonal vectors perpendicular to \mathbf{n} [57]. Following the same derivation as before, we obtain the Floquet Hamiltonian for the driven system:

$$\mathcal{H}_{\text{eff}}^{3D}(\mathbf{k}) = \sum_{\mu=\{x,y,z\}} \tilde{t}_\mu \cos k_\mu \sigma_\mu + t_- J_0(A_1) \sin k_x \sigma_y + M s_z \sigma_z + [F_y \sin k_y + F_z \sin k_z] \cos k_x \sigma_z. \quad (8)$$

For convenience, we have introduced the following shorthand notations: $\tilde{t}_x = t_+ J_0(A_1)$, $\tilde{t}_y = 2t_2 J_0(A_2)$, $\tilde{t}_z = 2t_3 J_0(A_3)$, $F_y = 8J_1(A_1)J_1(A_2)t_- t_2 \sin(\phi_2 - \phi_1)/\omega$, $F_z = 8J_1(A_1)J_1(A_3)t_- t_3 \sin \phi_1/\omega$, where $A_i = \lambda_i A_0$, $\lambda_1 = \sqrt{1 - \cos^2 \phi \sin^2 \theta}$, $\lambda_2 = \sqrt{1 - \sin^2 \phi \sin^2 \theta}$, $\lambda_3 = \eta \sin \theta$, $\phi_1 = \arg[\eta \cos \phi \cos \theta + i \sin \phi]$, and $\phi_2 = \arg[\eta \sin \phi \cos \theta - i \cos \phi]$. Despite the added complexity introduced by general-angle incidence, the resulting spin-splitting features and band topology remain straightforward to analyze.

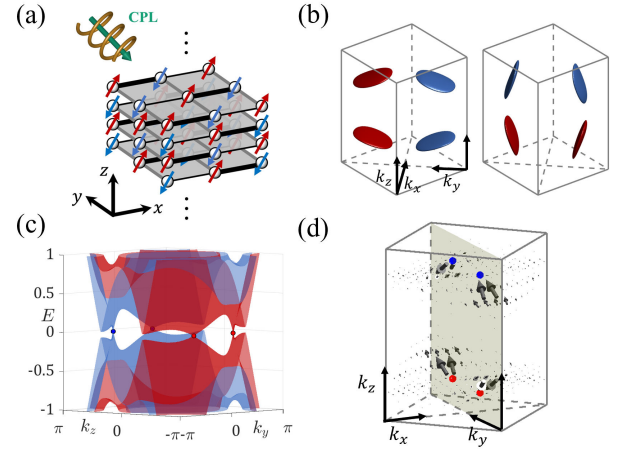


FIG. 4. (a) Realization of the 3D system through AB stacking. (b) Fermi surfaces at $E_F = 0.8$ for spin up (red) and spin down (blue), under CPL incident along the z (left) and y (right) directions. (c) Energy spectrum in the $k_x = 0$ plane, showing two Weyl points of each spin. (d) Berry curvature vector field across the Brillouin zone. The arrows' direction and magnitude represent the local Berry curvature. The value $M = 1$ is used in (b), and $M = 0.4$ is used in (c) and (d). Other shared parameters are $t_0 = 1$, $t_1 = 0.2$, $t_2 = 0.5$, $t_3 = 2$, $\eta = 1$, $A_0 = 1.8$, and $\omega = 9$.

Given the apparent symmetry between k_y and k_z in the Hamiltonian, Fermi surfaces with opposite spins can now be shifted in opposite directions along any axis in the k_y - k_z plane. To illustrate this symmetry, we plot the spin-split Fermi surfaces under CPL incident along the y and z directions. As shown in Fig. 4(b), Fermi surfaces with opposite spins exhibit opposite displacements: along the z direction for y -propagating CPL, and along the y direction for z -propagating CPL. Notably, when CPL propagates along any direction in the yz plane, the dimerization axis, the light propagation direction, and the Fermi surface displacement direction form an approximately orthogonal triad.

In our 2D system, we demonstrate that a Chern insulator emerges when the CPL amplitude surpasses a critical threshold. Stacking such Chern insulators can produce either 3D Chern insulators (for weak interlayer coupling) or Weyl semimetals (for strong coupling). Here, we focus on the realization of Weyl semimetals. From the 3D Hamiltonian [Eq. (8)], Weyl points emerge in the $k_x = 0$ plane when the CPL amplitude surpasses another critical threshold. Their positions are determined by: $\tilde{t}_x + \tilde{t}_y \cos k_y + \tilde{t}_z \cos k_z = 0$ and $sM + F_y \sin k_y + F_z \sin k_z = 0$ ($s = \pm 1$ for spin up/down). This system contains a minimum of four Weyl points, mirroring the situation in noncentrosymmetric Weyl semimetals with TRS [93]. Notably, although the unitary $[C_{2\perp} \parallel \mathcal{P}]$ symmetry constrains Weyl point locations identically to antiunitary TRS, it imposes opposite rules on the monopole charges of symmetry-related points. Specifically, Weyl points related by $[C_{2\perp} \parallel \mathcal{P}]$ carry opposite charges, whereas those related by TRS carry the same charge.

To demonstrate our analysis, we consider the simplified

case of y -direction ($\phi = \theta = \pi/2$) right-handed ($\eta = 1$) CPL incidence for clarity. In this configuration, the possible spin-up Weyl points are located at $\mathbf{k}_{w1} = (0, k_y^+, k_z^w)$, $\mathbf{k}_{w2} = (0, -k_y^+, k_z^w)$, $\mathbf{k}_{w3} = (0, k_y^-, \pi - k_z^w)$, $\mathbf{k}_{w4} = (0, -k_y^-, \pi - k_z^w)$, where $k_z^w = -\arcsin(M/F_z)$, and $k_y^\pm = \pi - \arccos[(\tilde{t}_x \pm \tilde{t}_z \cos k_z^w)/\tilde{t}_y]$. By choosing the parameters such that $|\tilde{t}_x - \tilde{t}_z \cos k_z^w| < \tilde{t}_y < |\tilde{t}_x + \tilde{t}_z \cos k_z^w|$, only the two Weyl points at \mathbf{k}_{w3} and \mathbf{k}_{w4} are present. Correspondingly, there are two spin-down Weyl points located at $-\mathbf{k}_{w3}$ and $-\mathbf{k}_{w4}$. In Fig. 4(c), we plot the energy bands in the $k_x = 0$ plane, which clearly exhibit two Weyl cones in each spin sector. Furthermore, Fig. 4(d) shows the distribution of Berry curvature vector field $\Omega(\mathbf{k}) = (\Omega_x(\mathbf{k}), \Omega_y(\mathbf{k}), \Omega_z(\mathbf{k}))$, where $\Omega_a(\mathbf{k}) = \sum_{E_n < 0} i\epsilon_{abc} \langle \partial_{k_b} u_n | \partial_{k_c} u_n \rangle$. Here ϵ_{abc} is the Levi-Civita symbol and $|u_n(\mathbf{k})\rangle$ is the eigenstate of the n -th occupied band. The field clearly reveals that inversion-related Weyl points act as a source and a sink of Berry flux, confirming they carry opposite monopole charges [93].

Discussions and conclusions.—We demonstrate that CPL can dynamically induce odd-parity altermagnetism in collinear \mathcal{PT} -symmetric antiferromagnets on dimerized lattices. The resulting odd-parity altermagnetic phase inherently supports topological states due to the underlying Dirac band structure. Remarkably, these systems also host favorable conditions for the emergence of unconventional superconductivity, as their band structure mimics time-reversal-invariant systems with SOC while explicitly breaking TRS. The fundamental relation $E(\mathbf{k}, s) = E(-\mathbf{k}, -s)$ ensures that a spin-up electron always has a spin-down partner available for pairing. This opens the door to realizing exotic, time-reversal-breaking spin-singlet superconductors.

Antiferromagnets on dimerized lattices correspond to systems exhibiting coexisting bond order and antiferromagnetic order. The bond order typically arises from electron-phonon interactions, whereas the antiferromagnetic order is driven by strong electron-electron repulsion. Their coexistence has been rigorously established through numerical studies of strongly correlated systems [89]. Beyond correlated materials, cold-atom systems offer a promising alternative platform for realizing our proposed odd-parity AMs. In such systems, the dimerized lattice can be directly engineered through optical lattice design [94], while the antiferromagnetic order can be stabilized by tuning the on-site interactions to be strongly repulsive [95–97]. The effect of CPL can be equivalently realized by periodically modulating the lattice [98].

To conclude, our work establishes a general dynamical protocol for creating odd-parity AMs, significantly expanding the class of systems capable of hosting these exotic phases and their emergent phenomena.

Acknowledgements.—This work is supported by the National Natural Science Foundation of China (Grant No. 12174455, No. 12474264), Guangdong Basic and Applied Basic Research Foundation (Grant No. 2023B1515040023), Guangdong Provincial Quantum Science Strategic Initiative (Grant No. GDZX2404007) and National Key R&D Program of China (Grant No. 2022YFA1404103).

* These authors contributed equally to this work.

† wuzhigang@quantumsc.cn

‡ yanzhb5@mail.sysu.edu.cn

- [1] L. Šmejkal, J. Sinova, and T. Jungwirth, Beyond Conventional Ferromagnetism and Antiferromagnetism: A Phase with Non-relativistic Spin and Crystal Rotation Symmetry, *Phys. Rev. X* **12**, 031042 (2022).
- [2] L. Šmejkal, J. Sinova, and T. Jungwirth, Emerging Research Landscape of Altermagnetism, *Phys. Rev. X* **12**, 040501 (2022).
- [3] L. Šmejkal, R. González-Hernández, T. Jungwirth, and J. Sinova, Crystal time-reversal symmetry breaking and spontaneous Hall effect in collinear antiferromagnets, *Science Advances* **6**, eaaz8809 (2020).
- [4] S. Hayami, Y. Yanagi, and H. Kusunose, Momentum-dependent spin splitting by collinear antiferromagnetic ordering, *Journal of the Physical Society of Japan* **88**, 123702 (2019).
- [5] S. Hayami, Y. Yanagi, and H. Kusunose, Bottom-up design of spin-split and reshaped electronic band structures in antiferromagnets without spin-orbit coupling: Procedure on the basis of augmented multipoles, *Phys. Rev. B* **102**, 144441 (2020).
- [6] L.-D. Yuan, Z. Wang, J.-W. Luo, E. I. Rashba, and A. Zunger, Giant momentum-dependent spin splitting in centrosymmetric low- Z antiferromagnets, *Phys. Rev. B* **102**, 014422 (2020).
- [7] L.-D. Yuan, Z. Wang, J.-W. Luo, and A. Zunger, Prediction of low- Z collinear and noncollinear antiferromagnetic compounds having momentum-dependent spin splitting even without spin-orbit coupling, *Phys. Rev. Mater.* **5**, 014409 (2021).
- [8] I. I. Mazin, K. Koepernik, M. D. Johannes, R. González-Hernández, and L. Šmejkal, Prediction of unconventional magnetism in doped FeSb₂, *Proceedings of the National Academy of Sciences* **118**, e2108924118 (2021).
- [9] D.-F. Shao, S.-H. Zhang, M. Li, C.-B. Eom, and E. Y. Tsymlal, Spin-neutral currents for spintronics, *Nature Communications* **12**, 7061 (2021).
- [10] H.-Y. Ma, M. Hu, N. Li, J. Liu, W. Yao, J.-F. Jia, and J. Liu, Multifunctional antiferromagnetic materials with giant piezomagnetism and noncollinear spin current, *Nature Communications* **12**, 2846 (2021).
- [11] P. Liu, J. Li, J. Han, X. Wan, and Q. Liu, Spin-group symmetry in magnetic materials with negligible spin-orbit coupling, *Phys. Rev. X* **12**, 021016 (2022).
- [12] X. Chen, J. Ren, Y. Zhu, Y. Yu, A. Zhang, P. Liu, J. Li, Y. Liu, C. Li, and Q. Liu, Enumeration and Representation Theory of Spin Space Groups, *Phys. Rev. X* **14**, 031038 (2024).
- [13] Z. Xiao, J. Zhao, Y. Li, R. Shindou, and Z.-D. Song, Spin Space Groups: Full Classification and Applications, *Phys. Rev. X* **14**, 031037 (2024).
- [14] Y. Jiang, Z. Song, T. Zhu, Z. Fang, H. Weng, Z.-X. Liu, J. Yang, and C. Fang, Enumeration of Spin-Space Groups: Toward a Complete Description of Symmetries of Magnetic Orders, *Phys. Rev. X* **14**, 031039 (2024).
- [15] T. Osumi, S. Souma, T. Aoyama, K. Yamauchi, A. Honma, K. Nakayama, T. Takahashi, K. Ohgushi, and T. Sato, Observation of a giant band splitting in altermagnetic MnTe, *Phys. Rev. B* **109**, 115102 (2024).
- [16] S. Lee, S. Lee, S. Jung, J. Jung, D. Kim, Y. Lee, B. Seok, J. Kim, B. G. Park, L. Šmejkal, C.-J. Kang, and C. Kim, Broken Kramers Degeneracy in Altermagnetic MnTe, *Phys. Rev. Lett.* **132**, 036702 (2024).
- [17] J. Krempaský, L. Šmejkal, S. W. D'Souza, M. Hajlaoui, G. Springholz, K. Uhlířová, F. Alarab, P. C. Constantinou,

- V. Strocov, D. Usanov, W. R. Pudello, R. González-Hernández, A. Birk Hellenes, Z. Jansa, H. Reichlová, Z. Šobáň, R. D. Gonzalez Betancourt, P. Wadley, J. Sinova, D. Kriegner, J. Minár, J. H. Dil, and T. Jungwirth, Altermagnetic lifting of Kramers spin degeneracy, *Nature* **626**, 517 (2024).
- [18] M. Hajlaoui, S. Wilfred D'Souza, L. Šmejkal, D. Kriegner, G. Krizman, T. Zakuslyo, N. Olszowska, O. Caha, J. Michalička, J. Sánchez-Barriga, A. Marmodoro, K. Výborný, A. Ernst, M. Cinchetti, J. Minar, T. Jungwirth, and G. Springholz, Temperature dependence of relativistic valence band splitting induced by an altermagnetic phase transition, *Advanced Materials* **36**, 2314076 (2024).
- [19] S. Reimers, L. Odenbreit, L. Šmejkal, V. N. Strocov, P. Constantinou, A. B. Hellenes, R. Jaeschke Ubierno, W. H. Campos, V. K. Bharadwaj, A. Chakraborty, T. Denneulin, W. Shi, R. E. Dunin-Borkowski, S. Das, M. Kläui, J. Sinova, and M. Jourdan, Direct observation of altermagnetic band splitting in CrSb thin films, *Nature Communications* **15**, 2116 (2024).
- [20] J. Ding, Z. Jiang, X. Chen, Z. Tao, Z. Liu, T. Li, J. Liu, J. Sun, J. Cheng, J. Liu, Y. Yang, R. Zhang, L. Deng, W. Jing, Y. Huang, Y. Shi, M. Ye, S. Qiao, Y. Wang, Y. Guo, D. Feng, and D. Shen, Large Band Splitting in g -Wave Altermagnet CrSb, *Phys. Rev. Lett.* **133**, 206401 (2024).
- [21] G. Yang, Z. Li, S. Yang, J. Li, H. Zheng, W. Zhu, Z. Pan, Y. Xu, S. Cao, W. Zhao, A. Jana, J. Zhang, M. Ye, Y. Song, L.-H. Hu, L. Yang, J. Fujii, I. Vobornik, M. Shi, H. Yuan, Y. Zhang, Y. Xu, and Y. Liu, Three-dimensional mapping of the altermagnetic spin splitting in CrSb, *Nature Communications* **16**, 1442 (2025).
- [22] M. Zeng, M.-Y. Zhu, Y.-P. Zhu, X.-R. Liu, X.-M. Ma, Y.-J. Hao, P. Liu, G. Qu, Y. Yang, Z. Jiang, K. Yamagami, M. Arita, X. Zhang, T.-H. Shao, Y. Dai, K. Shimada, Z. Liu, M. Ye, Y. Huang, Q. Liu, and C. Liu, Observation of Spin Splitting in Room-Temperature Metallic Antiferromagnet CrSb, *Advanced Science* **11**, 2406529 (2024).
- [23] C. Li, M. Hu, Z. Li, Y. Wang, W. Chen, B. Thiagarajan, M. Leandersson, C. Polley, T. Kim, H. Liu, C. Fulga, M. G. Vergniory, O. Janson, O. Tjernberg, and J. van den Brink, Topological Weyl altermagnetism in CrSb, *Communications Physics* **8**, 311 (2025).
- [24] B. Jiang, M. Hu, J. Bai, Z. Song, C. Mu, G. Qu, W. Li, W. Zhu, H. Pi, Z. Wei, Y.-J. Sun, Y. Huang, X. Zheng, Y. Peng, L. He, S. Li, J. Luo, Z. Li, G. Chen, H. Li, H. Weng, and T. Qian, A metallic room-temperature d -wave altermagnet, *Nature Physics* **21**, 754 (2025).
- [25] J. A. Ouassou, A. Brataas, and J. Linder, dc Josephson Effect in Altermagnets, *Phys. Rev. Lett.* **131**, 076003 (2023).
- [26] C. Sun, A. Brataas, and J. Linder, Andreev reflection in altermagnets, *Phys. Rev. B* **108**, 054511 (2023).
- [27] M. Papaj, Andreev reflection at the altermagnet-superconductor interface, *Phys. Rev. B* **108**, L060508 (2023).
- [28] C. W. J. Beenakker and T. Vakhtel, Phase-shifted Andreev levels in an altermagnet Josephson junction, *Phys. Rev. B* **108**, 075425 (2023).
- [29] Q. Cheng and Q.-F. Sun, Orientation-dependent Josephson effect in spin-singlet superconductor/altermagnet/spin-triplet superconductor junctions, *Phys. Rev. B* **109**, 024517 (2024).
- [30] B. Lu, K. Maeda, H. Ito, K. Yada, and Y. Tanaka, φ Josephson Junction Induced by Altermagnetism, *Phys. Rev. Lett.* **133**, 226002 (2024).
- [31] S.-B. Zhang, L.-H. Hu, and T. Neupert, Finite-momentum Cooper pairing in proximitized altermagnets, *Nature Communications* **15**, 1801 (2024).
- [32] S. Sumita, M. Naka, and H. Seo, Fulde-Ferrell-Larkin-Ovchinnikov state induced by antiferromagnetic order in κ -type organic conductors, *Phys. Rev. Res.* **5**, 043171 (2023).
- [33] D. Chakraborty and A. M. Black-Schaffer, Zero-field finite-momentum and field-induced superconductivity in altermagnets, *Phys. Rev. B* **110**, L060508 (2024).
- [34] G. Sim and J. Knolle, Pair density waves and supercurrent diode effect in altermagnets, *Phys. Rev. B* **112**, L020502 (2025).
- [35] Z. Liu, H. Hu, and X.-j. Liu, Fulde-Ferrell-Larkin-Ovchinnikov States and Topological Bogoliubov Fermi Surfaces in Altermagnets: an Analytical Study, *arXiv e-prints*, arXiv:2508.07813 (2025).
- [36] B. Brekke, A. Brataas, and A. Sudbø, Two-dimensional altermagnets: Superconductivity in a minimal microscopic model, *Phys. Rev. B* **108**, 224421 (2023).
- [37] K. Mæland, B. Brekke, and A. Sudbø, Many-body effects on superconductivity mediated by double-magnon processes in altermagnets, *Phys. Rev. B* **109**, 134515 (2024).
- [38] A. Bose, S. Vadrnais, and A. Paramekanti, Altermagnetism and superconductivity in a multiorbital $t - J$ model, *Phys. Rev. B* **110**, 205120 (2024).
- [39] V. S. de Carvalho and H. Freire, Unconventional superconductivity in altermagnets with spin-orbit coupling, *Phys. Rev. B* **110**, L220503 (2024).
- [40] N. Parthenios, P. M. Bonetti, R. González-Hernández, W. H. Campos, L. Šmejkal, and L. Classen, Spin and pair density waves in 2D altermagnetic metals, *arXiv e-prints*, arXiv:2502.19270 (2025).
- [41] K. Maeda, Y. Fukaya, K. Yada, B. Lu, Y. Tanaka, and J. Cayao, Classification of pair symmetries in superconductors with unconventional magnetism, *Phys. Rev. B* **111**, 144508 (2025).
- [42] S. Hong, M. J. Park, and K.-M. Kim, Unconventional p -wave and finite-momentum superconductivity induced by altermagnetism through the formation of bogoliubov fermi surface, *Phys. Rev. B* **111**, 054501 (2025).
- [43] K. Parshukov and A. P. Schnyder, Exotic superconducting states in altermagnets, *arXiv e-prints*, arXiv:2507.10700 (2025).
- [44] Y.-M. Wu, Y. Wang, and R. M. Fernandes, Intra-unit-cell singlet pairing mediated by altermagnetic fluctuations, *arXiv e-prints*, arXiv:2506.04356 (2025).
- [45] D. Zhu, Z.-Y. Zhuang, Z. Wu, and Z. Yan, Topological superconductivity in two-dimensional altermagnetic metals, *Phys. Rev. B* **108**, 184505 (2023).
- [46] D. Zhu, D. Liu, Z.-Y. Zhuang, Z. Wu, and Z. Yan, Field-sensitive dislocation bound states in two-dimensional d -wave altermagnets, *Phys. Rev. B* **110**, 165141 (2024).
- [47] Y.-X. Li and C.-C. Liu, Majorana corner modes and tunable patterns in an altermagnet heterostructure, *Phys. Rev. B* **108**, 205410 (2023).
- [48] Y.-X. Li, Y. Liu, and C.-C. Liu, Creation and manipulation of higher-order topological states by altermagnets, *Phys. Rev. B* **109**, L201109 (2024).
- [49] S. A. A. Ghorashi, T. L. Hughes, and J. Cano, Altermagnetic Routes to Majorana Modes in Zero Net Magnetization, *Phys. Rev. Lett.* **133**, 106601 (2024).
- [50] P. Rao, A. Mook, and J. Knolle, Tunable band topology and optical conductivity in altermagnets, *Phys. Rev. B* **110**, 024425 (2024).
- [51] H.-Y. Ma and J.-F. Jia, Altermagnetic topological insulator and the selection rules, *Phys. Rev. B* **110**, 064426 (2024).
- [52] D. S. Antonenko, R. M. Fernandes, and J. W. F. Venderbos, Mirror Chern Bands and Weyl Nodal Loops in Altermagnets, *Phys. Rev. Lett.* **134**, 096703 (2025).
- [53] S. Qu, X.-Y. Hou, Z.-X. Liu, P.-J. Guo, and Z.-Y. Lu, Altermagnetic Weyl node-network metals protected by spin symmetry,

- Phys. Rev. B **111**, 195138 (2025).
- [54] K. Parshukov, R. Wiedmann, and A. P. Schnyder, Topological crossings in two-dimensional altermagnets: Symmetry classification and topological responses, Phys. Rev. B **111**, 224406 (2025).
 - [55] R. M. Fernandes, V. S. de Carvalho, T. Birol, and R. G. Pereira, Topological transition from nodal to nodeless Zeeman splitting in altermagnets, Phys. Rev. B **109**, 024404 (2024).
 - [56] Z.-Y. Zhuang, D. Zhu, Z. Wu, and Z. Yan, Cartesian Nodal Lines and Magnetic Kramers Weyl Nodes in Spin-Split Antiferromagnets, arXiv e-prints, arXiv:2502.13212 (2025).
 - [57] D. Liu, Z.-Y. Zhuang, and Z. Yan, Floquet-Engineering Weyl Points and Linked Fermi Arcs from Straight Nodal Lines, arXiv e-prints, arXiv:2507.04489 (2025).
 - [58] J. E. Hirsch, Spin-split states in metals, Phys. Rev. B **41**, 6820 (1990).
 - [59] J. E. Hirsch, Chromium: A possible spin-split metal, Phys. Rev. B **41**, 6828 (1990).
 - [60] L. P. Gor'kov and A. Sokol, Nontrivial magnetic order: Localized versus itinerant systems, Phys. Rev. Lett. **69**, 2586 (1992).
 - [61] C. M. Varma and L. Zhu, Helicity Order: Hidden Order Parameter in URu₂Si₂, Phys. Rev. Lett. **96**, 036405 (2006).
 - [62] C. Wu and S.-C. Zhang, Dynamic generation of spin-orbit coupling, Phys. Rev. Lett. **93**, 036403 (2004).
 - [63] C. Wu, K. Sun, E. Fradkin, and S.-C. Zhang, Fermi liquid instabilities in the spin channel, Phys. Rev. B **75**, 115103 (2007).
 - [64] E. I. Kiselev, M. S. Scheurer, P. Wölfle, and J. Schmalian, Limits on dynamically generated spin-orbit coupling: Absence of $l = 1$ Pomeranchuk instabilities in metals, Phys. Rev. B **95**, 125122 (2017).
 - [65] Y.-M. Wu, A. Klein, and A. V. Chubukov, Conditions for $l = 1$ Pomeranchuk instability in a Fermi liquid, Phys. Rev. B **97**, 165101 (2018).
 - [66] A. Birk Hellenes, T. Jungwirth, R. Jaeschke-Ubiergo, A. Chakraborty, J. Sinova, and L. Šmejkal, P-wave magnets, arXiv e-prints, arXiv:2309.01607 (2023).
 - [67] Y. Yu, M. B. Lyngby, T. Shishidou, M. Roig, A. Kreisel, M. Weinert, B. M. Andersen, and D. F. Agterberg, Odd-Parity Magnetism Driven by Antiferromagnetic Exchange, Phys. Rev. Lett. **135**, 046701 (2025).
 - [68] Q. Song, S. Stavić, P. Barone, A. Droghetti, D. S. Antonenko, J. W. F. Venderbos, C. A. Occhialini, B. Ilyas, E. Ergeçen, N. Gedik, S.-W. Cheong, R. M. Fernandes, S. Picozzi, and R. Comin, Electrical switching of a p-wave magnet, Nature **642**, 64 (2025).
 - [69] B. Brekke, P. Sukhachov, H. G. Giil, A. Brataas, and J. Linder, Minimal models and transport properties of unconventional p-wave magnets, Phys. Rev. Lett. **133**, 236703 (2024).
 - [70] S. Xu, M. Yang, Y. Li, B. Shen, S. Gong, J. Huang, P. Yu, Y. Li, and J. Luo, Spin symmetry study in non-collinear CrSe: Odd-wave magnetism induced by glide mirror symmetry breaking, Applied Physics Letters **127**, 032407 (2025).
 - [71] Y.-P. Lin, Odd-parity altermagnetism through sublattice currents: From Haldane-Hubbard model to general bipartite lattices, arXiv e-prints, arXiv:2503.09602 (2025).
 - [72] F. D. M. Haldane, Model for a quantum Hall effect without landau levels: Condensed-matter realization of the “parity anomaly”, Phys. Rev. Lett. **61**, 2015 (1988).
 - [73] T. Oka and H. Aoki, Photovoltaic Hall effect in graphene, Phys. Rev. B **79**, 081406 (2009).
 - [74] T. Kitagawa, T. Oka, A. Brataas, L. Fu, and E. Demler, Transport properties of nonequilibrium systems under the application of light: Photoinduced quantum hall insulators without landau levels, Phys. Rev. B **84**, 235108 (2011).
 - [75] Z. Gu, H. A. Fertig, D. P. Arovas, and A. Auerbach, Floquet spectrum and transport through an irradiated graphene ribbon, Phys. Rev. Lett. **107**, 216601 (2011).
 - [76] J. Cayssol, B. Dóra, F. Simon, and R. Moessner, Floquet topological insulators, physica status solidi (RRL)-Rapid Research Letters **7**, 101 (2013).
 - [77] G. Usaj, P. M. Perez-Piskunow, L. E. F. Foa Torres, and C. A. Balseiro, Irradiated graphene as a tunable Floquet topological insulator, Phys. Rev. B **90**, 115423 (2014).
 - [78] R. Wang, B. Wang, R. Shen, L. Sheng, and D. Xing, Floquet Weyl semimetal induced by off-resonant light, Europhysics Letters **105**, 17004 (2014).
 - [79] H. Hübener, M. A. Sentef, U. De Giovannini, A. F. Kemper, and A. Rubio, Creating stable Floquet-Weyl semimetals by laser-driving of 3D Dirac materials, Nature Communications **8**, 13940 (2017).
 - [80] Z. Yan and Z. Wang, Tunable Weyl Points in Periodically Driven Nodal Line Semimetals, Phys. Rev. Lett. **117**, 087402 (2016).
 - [81] C.-K. Chan, Y.-T. Oh, J. H. Han, and P. A. Lee, Type-II Weyl cone transitions in driven semimetals, Phys. Rev. B **94**, 121106 (2016).
 - [82] A. Narayan, Tunable point nodes from line-node semimetals via application of light, Phys. Rev. B **94**, 041409 (2016).
 - [83] Z. Yan and Z. Wang, Floquet multi-Weyl points in crossing-nodal-line semimetals, Phys. Rev. B **96**, 041206 (2017).
 - [84] M. Ezawa, Photoinduced topological phase transition from a crossing-line nodal semimetal to a multiple-Weyl semimetal, Phys. Rev. B **96**, 041205 (2017).
 - [85] S. Huang, Z. Qin, F. Zhan, D.-H. Xu, D.-S. Ma, and R. Wang, Light-induced Odd-parity Magnetism in Conventional Collinear Antiferromagnets, arXiv e-prints, arXiv:2507.20705 (2025).
 - [86] B. Li, D.-F. Shao, and A. A. Kovalev, Floquet Spin Splitting and Spin Generation in Antiferromagnets, arXiv e-prints, arXiv:2507.22884 (2025).
 - [87] T. Zhu, D. Zhou, H. Wang, and J. Ruan, Floquet odd-parity collinear magnets, arXiv e-prints, arXiv:2508.02542 (2025).
 - [88] X. Cai, Z.-X. Li, and H. Yao, Antiferromagnetism Induced by Bond Su-Schrieffer-Heeger Electron-Phonon Coupling: A Quantum Monte Carlo Study, Phys. Rev. Lett. **127**, 247203 (2021).
 - [89] A. Tanjaroony Ly, B. Cohen-Stead, and S. Johnston, Antiferromagnetic and bond-order-wave phases in the half-filled two-dimensional optical Su-Schrieffer-Heeger-Hubbard model, Phys. Rev. B **111**, 245138 (2025).
 - [90] W. P. Su, J. R. Schrieffer, and A. J. Heeger, Solitons in Polyacetylene, Phys. Rev. Lett. **42**, 1698 (1979).
 - [91] N. Goldman and J. Dalibard, Periodically Driven Quantum Systems: Effective Hamiltonians and Engineered Gauge Fields, Phys. Rev. X **4**, 031027 (2014).
 - [92] X.-L. Qi, Y.-S. Wu, and S.-C. Zhang, Topological quantization of the spin Hall effect in two-dimensional paramagnetic semiconductors, Phys. Rev. B **74**, 085308 (2006).
 - [93] N. P. Armitage, E. J. Mele, and A. Vishwanath, Weyl and dirac semimetals in three-dimensional solids, Rev. Mod. Phys. **90**, 015001 (2018).
 - [94] M. Atala, M. Aidelsburger, J. T. Barreiro, D. Abanin, T. Kitagawa, E. Demler, and I. Bloch, Direct measurement of the Zak phase in topological Bloch bands, Nature Physics **9**, 795 (2013).
 - [95] R. A. Hart, P. M. Duarte, T.-L. Yang, X. Liu, T. Paiva, E. Khatami, R. T. Scalettar, N. Trivedi, D. A. Huse, and R. G. Hulet, Observation of antiferromagnetic correlations in the Hubbard model with ultracold atoms, Nature **519**, 211 (2015).

- [96] A. Mazurenko, C. S. Chiu, G. Ji, M. F. Parsons, M. Kanász-Nagy, R. Schmidt, F. Grusdt, E. Demler, D. Greif, and M. Greiner, A cold-atom fermi-hubbard antiferromagnet, *Nature* **545**, 462 (2017).
- [97] H.-J. Shao, Y.-X. Wang, D.-Z. Zhu, Y.-S. Zhu, H.-N. Sun, S.-Y. Chen, C. Zhang, Z.-J. Fan, Y. Deng, X.-C. Yao, Y.-A. Chen, and J.-W. Pan, Antiferromagnetic phase transition in a 3D fermionic Hubbard model, *Nature* **632**, 267 (2024).
- [98] G. Jotzu, M. Messer, R. Desbuquois, M. Lebrat, T. Uehlinger, D. Greif, and T. Esslinger, Experimental realization of the topological Haldane model with ultracold fermions, *Nature* **515**, 237 (2014).